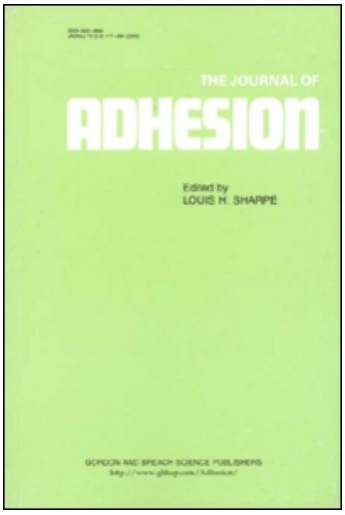

The Journal of Adhesion
Publication details, including instructions for authors and subscription information:
http://www.informaworld.com/smpp/title~content=t713453635

SURFACTANT ADSORPTION TO SPHERICAL PARTICLES: THE INTRINSIC LENGTH SCALE GOVERNING THE SHIFT FROM DIFFUSION TO KINETIC-CONTROLLED MASS TRANSFER

Fang Jin[a]; R. Balasubramaniam[b]; Kathleen J. Stebe[c]
[a] Department of Chemical & Biomolecular Engineering, Johns Hopkins University, Baltimore, Maryland, USA [b] NASA Glenn Research Center, Cleveland, Ohio, USA [c] Department of Chemical & Biomolecular Engineering, Department of Materials Science & Engineering, Department of Mechanical Engineering, Department of Biomedical Engineering, Johns Hopkins University, Baltimore, Maryland, USA

Online publication date: 10 August 2010

To cite this Article Jin, Fang , Balasubramaniam, R. and Stebe, Kathleen J.(2004) 'SURFACTANT ADSORPTION TO SPHERICAL PARTICLES: THE INTRINSIC LENGTH SCALE GOVERNING THE SHIFT FROM DIFFUSION TO KINETIC-CONTROLLED MASS TRANSFER', The Journal of Adhesion, 80: 9, 773 — 796
To link to this Article: DOI: 10.1080/00218460490480770
URL: http://dx.doi.org/10.1080/00218460490480770

The Journal of Adhesion, 80: 773–796, 2004

ISSN: 0021-8464 print/1545-5823 online
DOI: 10.1080/00218460490480770

Taylor & Francis
Taylor & Francis Group

SURFACTANT ADSORPTION TO SPHERICAL PARTICLES: THE INTRINSIC LENGTH SCALE GOVERNING THE SHIFT FROM DIFFUSION TO KINETIC-CONTROLLED MASS TRANSFER

Fang Jin
Department of Chemical & Biomolecular Engineering,
Johns Hopkins University, Baltimore, Maryland, USA

R. Balasubramaniam
NASA Glenn Research Center, Cleveland, Ohio, USA

Kathleen J. Stebe
Department of Chemical & Biomolecular Engineering,
Department of Materials Science & Engineering,
Department of Mechanical Engineering,
Department of Biomedical Engineering,
Johns Hopkins University, Baltimore, Maryland, USA

When a drop or bubble of radius b is formed in surfactant solution, surfactant adsorbs, diffuses from solution, and desorbs to establish the equilibrium surface concentration. The transport coefficients for diffusion, adsorption, and desorption are fundamental parameters. However, the transport mechanisms that control the interface far from equilibrium are highly context dependent. Thus, no surfactant has universal "diffusion-controlled" transport. Here we identify a new length scale, $R_{D\text{-}K}$, that depends on surfactant physicochemistry, and which ranges from roughly 15 to 65 microns. For drops or bubbles with $b \ll R_{D\text{-}K}$, mass transfer is kinetically controlled. For $b \gg R_{D\text{-}K}$, mass transfer is diffusion controlled. Simulations of adsorption to quiescent spherical interfaces support the importance of $R_{D\text{-}K}$ in determining the controlling transport mechanism for surfactant solutions with concentrations below the critical micelle concentration (CMC). While the case

Received 23 January 2004; in final form 22 April 2004.

One of a collection of papers honoring A. W. Neumann, the recipient in February 2004 of *The Adhesion Society Award for Excellence in Adhesion Science, Sponsored by 3M*.

This work was supported by NASA's Physical Science Research Division through grant NCC3-812 from NASA Glenn Research Center to Johns Hopkins University.

Address correspondence to Kathleen J. Stebe, Department of Chemical and Biomolecular Engineering, Johns Hopkins University, 3400 North Charles Street, Baltimore, MD 21218, USA. E-mail: kjs@jhu.edu

of surfactant adsorbing to a bubble is discussed in detail, the arguments presented are quite general and should apply to adsorption of any solute to any spherical particle.

Keywords: Dynamic surface tension; Microfluidics; Capping agents

INTRODUCTION

Surface tension evolutions of pendant drops or bubbles are analyzed to find the transport kinetic constants that determine the rates of surfactant diffusion, adsorption, and desorption. When drops or bubbles are formed in surfactant solutions and moved by applied fields (be they applied pressure fields, gravity, or electric fields), these transport coefficients must be understood to predict drop or bubble behavior. The transport coefficients for diffusion, adsorption, and desorption are fundamental parameters that are independent of the context in which they are applied. However, the transport mechanisms that control the interface far from equilibrium are highly context dependent. Thus, it is incorrect to state that a surfactant has universally "diffusion-controlled" transport without addressing the drop radius and prevailing solution conditions (*e.g.*, absence or presence of flow, and analyses of relative rates of adsorption and desorption). Here we develop a scaling argument to identify a characteristic length scale for surfactant adsorption, $R_{D\text{-}K}$. For quiescent drops or bubbles with radii smaller than $R_{D\text{-}K}$, mass transfer is kinetically controlled. For radii larger than $R_{D\text{-}K}$, mass transfer is diffusion controlled.

The shape of a pendant drop or bubble is determined by gravity, which distends the bubble, and surface tension, which resists this deformation. The balance of these forces is expressed in the Young-Laplace equation, which in scaled form contains the Bond number

$$Bo = \frac{\Delta\rho g b^2}{\gamma}, \tag{1}$$

where $\Delta\rho$ is a density difference between the drop or bubble and the suspending fluid, g is the gravitational constant, b is the drop or bubble radius, and γ is the surface tension. When Bo is sufficiently large, the distension of the drop or bubble shape by gravity is sufficiently pronounced so that shapes differ with surface tension. In this circumstance, numerical solutions of the Young-Laplace equation can be compared with observed shapes to determine the surface tension. A major advance in this technique was made when Rotenberg *et al.* [1] recognized that drop or bubble silhouettes could be obtained using

digital cameras and analyzed rapidly and precisely. Bubble radii are always limited to approximately 10^{-3} m in pendant bubble studies for aqueous systems, owing to the requirement that the bubble be large enough for gravity to distend it but small enough that surface tension forces along the three-phase contact line remain sufficiently strong to retain the bubble on the needle. Thus, most pendant bubble analyses are performed for *Bo* of roughly 0.15 (*e.g.*, see previous pendant bubble studies [2–10]). Similar restrictions emerge for drops. Because of this, the impact of drop or bubble radius on the controlling surfactant mass transfer regime has not been explored in dynamic surface tension experiments. With the advent of microfluidics, in which drops and bubbles of submillimeter-to submicron-length scales are formed and manipulated, the importance of understanding the influence of bubble or drop radius is increasing [11]. At these reduced radii, the mass transfer mechanisms that govern surface tension evolution change, simply because of the dependence of bulk Fickian diffusional fluxes on geometry. This effect is the focus of this article, in which drops or bubbles are sufficiently small so that their curvature is significant in the surfactant Fickian diffusion flux but sufficiently large compared with molecular dimensions so that curvature-related corrections need not be made to the definition of the surface tension or to the adsorption isotherm. The arguments are general and can be extended to adsorption to solid particles. While the ideas presented here can be extended to micellar systems, our discussions and numerical simulations are limited to concentrations below the critical micelle concentration (CMC).

The pendant bubble technique has been adopted to study dynamic surface tension by recording bubble shapes from the time of formation in a surfactant solution until they have attained equilibrium, providing detailed surface tension evolutions under hydrostatic conditions that are suitable for analysis in terms of the surfactant mass transfer dynamics and surfactant thermodynamics, (see earlier reviews [2–5], as well as the literature reviews in Pan *et al.* [6] and Lee *et al.* [7]). These studies have improved our understanding of dynamic surface tension in terms of bulk diffusion, adsorption–desorption kinetics, and intermolecular interactions among adsorbed surfactants. Two important ideas have been exploited to provide this deeper understanding. The first is the existence of a characteristic length scale over which bulk diffusion occurs for adsorption to a surface, termed the adsorption depth h, discussed in detail in Ferri and Stebe [5]. The second is the concept of a shift in mass transfer mechanism controlling the rate of surface tension reduction with increasing bulk concentration, even at concentrations below the CMC [6, 8–10]. In the following paragraphs, both concepts are reviewed briefly for planar interfaces. The role of drop or bubble radius,

explored in prior work in the diffusion-controlled limit [12], is then more fully discussed, and the new intrinsic length scale is introduced.

The adsorption depth, h, can be understood by considering the adsorption of surfactant to a planar area element, dA. The mass adsorbed at equilibrium can be estimated as $\Gamma_{eq}\ dA$, where Γ_{eq} is the surface concentration of surfactant in equilibrium with the bulk concentration, C_∞. To estimate the depth depleted to supply the area element, dA, consider the mass in the volume element, dV, below the interface, $C_\infty dV = C_\infty h dA$. Equating this expression to the adsorbed mass, the adsorption depth can be found:

$$h = \Gamma_{eq}/C_\infty. \tag{2a}$$

The adsorption depth is a measure of the distances over which surfactant molecules must diffuse to supply the interface. For planar systems, h can be used to define a characteristic time required to supply surfactant to the interface by diffusion,

$$\tau_{D\,planar} = h^2/D, \tag{2b}$$

where D is the surfactant diffusivity. Because surfactant molecules have finite cross-sectional areas, there is an upper bound to the surface concentration, given by the maximum packing limit, Γ_∞. Thus, at high concentrations, h varies inversely with bulk concentration, and the characteristic diffusion time scale becomes rapid as concentration increases. The adsorption depth for common surfactants can be on the order of 10^{-1} m for dilute concentrations of surfactants and can reduce to between 10^{-5}–10^{-3} m for concentrations approaching the CMC [5].

When a planar fluid interface is formed in a surfactant solution, surfactant adjacent to the interface adsorbs, depleting the solution immediately below the surface. Surfactants diffuse from the bulk to supply this depleted region. At long times, the diffusion flux slows as the surface concentration approaches equilibrium, and the rates of adsorption and desorption must balance. Thus, the rates of adsorption, desorption, and bulk diffusion all play a role in determining the surface tension evolution. Scaling arguments are presented here to motivate the numerical simulations performed in this article. The characteristic timescale for a purely diffusion-controlled flux to a planar interface is given in Equation (2b). The characteristic timescale for a purely adsorption-desorption–controlled flux (assuming Langmuirian kinetics) is given by

$$\tau_{ads-des} = \frac{1}{(\beta C_\infty + \alpha)}, \tag{3}$$

where βC_∞ is the characteristic collisional frequency for adsorption and α is the desorption kinetic constant. The ratio of the diffusion time scale to the adsorption–desorption time scale yields

$$\Lambda_{planar} = \frac{\alpha}{D}\frac{\Gamma_{eq}{}^2}{C_\infty{}^2}\left(\frac{\beta C_\infty}{\alpha} + 1\right). \tag{4}$$

This ratio determines the mechanism that controls the evolution of the surface tension in a planar system. If $\Lambda_{planar} \gg 1$, diffusion is rate limiting (*i.e.*, diffusion is relatively slow compared with adsorption–desorption kinetics). Conversely, if $\Lambda_{planar} \ll 1$, adsorption–desorption kinetics are rate limiting. It is also clear that Λ_{planar} depends strongly on the bulk concentration. At dilute concentrations, ($\frac{\beta C_\infty}{\alpha} \ll 1$) the surface concentration is related to the bulk concentration by a Henry's law slope, $\Gamma_{eq} \approx \Gamma_\infty \frac{\beta C_\infty}{\alpha}$, where Γ_∞ is the maximum packing of surfactant. At high concentration, ($\frac{\beta C_\infty}{\alpha} \gg 1$), Γ_{eq} approaches the maximum packing, Γ_∞, slowly from below. Using these limiting arguments, asymptotic forms for Λ_{planar} can be derived:

$$\Lambda_{dilute} = \frac{\beta^2}{D}\frac{\Gamma_\infty{}^2}{\alpha}, \tag{5a}$$

$$\Lambda_{concentrated} = \frac{\beta\Gamma_\infty}{D}\frac{\Gamma_\infty}{C_\infty} = \frac{\Lambda_{dilute}}{\frac{\beta C_\infty}{\alpha}}. \tag{5b}$$

Note that this delineation as *dilute* or *concentrated* is given in terms of $\frac{\beta C_\infty}{\alpha}$; the normalizing factor for concentration in this expression (α/β) is quite small (see recent reviews [2, 5, 6]; for example, α/β is 5×10^{-6} M for the Surfynol® acetylenic diol surfactant [13] and 2.5×10^{-8} M for $C_{12}E_6$ [6]). Simply, bulk concentrations for which the surface tension reduces by more than 5–10 mN/m from the clean interface value correspond to concentrated solutions, according to this argument. At dilute concentrations, the ratio of these time scales is independent of bulk concentration. However, for $\frac{\beta C_\infty}{\alpha} \gg 1$ (*i.e.*, the normal circumstance), Λ_{planar} varies inversely with concentration, indicating that diffusion becomes less important as concentration increases. Depending upon the values of the physicochemical constants in Equation (5b), the mass transfer mechanism can shift from one of diffusion control at dilute concentrations to kinetic control at higher concentrations (which can be well below the CMC). Arguments along these lines were developed independently by Pan *et al.* [6] and Lin and collaborators [8–10], and were used to guide pendant bubble experiments designed to determine the kinetic constants for adsorption and desorption for ethoxylated surfactants with structures C_nE_m, where C_n indicates a

saturated hydrocarbon chain of n carbons and E_m represents repeated ethoxy groups, $(-OCH_2CH_2)_m-OH$. Pan focused on the mass transfer of $C_{12}E_6$ and showed that this molecule's mass transfer indeed shifts from diffusion control at dilute concentrations to kinetic control at elevated bulk concentrations. Lin and collaborators have studied a series of ethoxylated surfactants; their results are summarized in Table 1.

When the adsorption depth is small compared with the bubble radius, b, the diffusional fluxes are well described by the planar arguments given above. However, since h can be as large as 10^{-1} m, the ratio $h/b \geq 1$ over a large range of concentrations. Under these conditions, diffusional mass flux is faster to the sphere than to a planar surface. A dimensional analysis on the surface mass balance equating the rate of adsorbed surfactant accumulation to the diffusion flux from solution to a spherical surface of radius b yields an amended characteristic time scale for diffusion:

$$\tau_{Dsphere} = hb/D. \tag{6}$$

The characteristic time for adsorption–desorption remains unchanged from Equation (3). Therefore, the ratio of these time scales becomes:

$$\Lambda_{sphere} = \frac{hb/D}{1/(\beta C_\infty + \alpha)}, \tag{7a}$$

which for a Langmuir model for Γ_{eq} simplifies for all concentrations to

$$\Lambda_{sphere} = \frac{b}{R_{D-K}}, \tag{7b}$$

where the intrinsic length scale, R_{D-K}, is defined:

$$R_{D-K} = \frac{D}{\beta \Gamma_\infty}. \tag{7c}$$

For $\Lambda_{sphere} \gg 1$, mass transfer to the sphere is diffusion controlled. For $\Lambda_{sphere} \ll 1$, mass transfer to the sphere is kinetically controlled. (Note that $\Lambda_{planar} = h/R_{D-K}$, so R_{D-K} is important even in the absence of

TABLE 1 $R_{D\text{-}K}$ for Various Surfactants

	Γ_∞ (mol/m^2) $\times 10^6$	β m^3/mol/s	D m^2/s $\times 10^{10}$	R_{D-K} (micron)
$C_{12}E_6$	3.5	4.0	6.0	42.9
$C_{14}E_8$	6.8	5.4	8.7	23.7
$C_{12}E_8$	2.7	4.6	8.0	65.2
$C_{10}E_8$	3.0	6.9	6.5	30.7
n-decanol	6.5	6.7	7.7	17.7

curvature.) The characteristic radius at which mass transfer to a drop or bubble shifts from diffusion controlled to kinetic control is defined as $R_{D\text{-}K}$. The collapse of the physicochemical scaling arguments into this simple-length scale is particularly powerful. It has been noted by Pan *et al.* [6] that the factor $\beta\Gamma_\infty$ varies weakly with surfactant type, with values ranging from roughly 10^{-4}–10^{-6} m/s for surface-active materials ranging from weakly surface-active short-chain alcohols to highly surface-active surfactants. The diffusivity, D, also varies weakly with surfactant type, because most nonpolymeric surfactants fall within a similar size range; D can usually be estimated as roughly $5 \times 10^{-10}\,\mathrm{m}^2/\mathrm{s}$. Therefore, R_{D-K} usually falls within the range of 5×10^{-6} to 5×10^{-4} m; values for R_{D-K} corresponding to a number of highly surface-active substances studied in the literature are reported in Table 1. For highly surface-active molecules, R_{D-K} can range from as high as 65 microns (for $C_{12}E_8$) to as low as 17 microns (for 1-decanol). Thus, highly surface-active molecules adsorbing to bubbles or drops with radii of roughly 10 microns or less should be kinetically controlled for all concentration ranges by this argument. While our main focus is on fluid interfaces, the adsorption and diffusion discussion presented is quite general and applies to adsorption to solid surfaces as well. Thus, these shifts in controlling mechanisms for mass transfer to spherical particle arguments presented here apply equally to solid particles and indicate that adsorption kinetics may dominate for all small particles.

In this article, the shifts in mechanism predicted by this scaling argument are confirmed for the example of the surfactant $C_{12}E_6$, whose adsorption and desorption kinetic constants, bulk diffusivity, and Frumkin parameters have been reported by Pan *et al.* [6] The evolutions of the surface tensions and surface concentrations are found by numerically integrating the equations governing mass transfer to a spherical bubble or drop of radius b with surfactant in the fluid external to the sphere using these kinetic constants. The evolutions predicted by the mixed kinetic-diffusion model are compared with those obtained by considering mass fluxes controlled either solely by diffusion or by the sorption kinetics.

SURFACTANT TRANSPORT TO A SPHERICAL BUBBLE

Two types of quiescent adsorption experiments can be performed for a bubble immersed in a surfactant solution. The bubble can be freshly formed in solution and surfactant can adsorb to reduce the surface tension to its equilibrium value. Or, a bubble already at equilibrium with its surroundings can be suddenly compressed to a surface

concentration greater than its equilibrium. The subsequent desorption of surfactant and increase in surface tension to equilibrium can be studied. The equations governing both cases are delineated here.

Mixed Controlled Adsorption to an Initially Surfactant-free Surface

A bubble of radius b is formed at $t = 0$ in a surfactant solution of far-field concentration, C_∞. It is assumed that all motion associated with the bubble formation dissipates rapidly compared with the mass transfer time scales, so convection is ignored. A spherical coordinate system is adopted. Since spherical symmetry is assumed, the concentration varies spatially only with radial coordinate r. The sublayer concentration, C_s, is defined as the concentration of surfactant in solution immediately adjacent to the interface, *i.e.*,

$$C_s(t) = C(r = b, t). \tag{8}$$

Initially, C_s is equal to C_∞, the bulk concentration profile is spatially uniform, and the surface concentration, Γ, is zero, *i.e.*,

$$C_s(t = 0) = C_\infty, \quad C(r, t = 0) = C_\infty, \quad \Gamma(t = 0) = 0. \tag{9}$$

The Frumkin model [14] is adopted to describe the adsorption–desorption flux of surfactant:

$$\frac{d\Gamma}{dt} = \beta\Gamma_\infty C_s\left(1 - \frac{\Gamma}{\Gamma_\infty}\right) - \alpha \exp(-K\Gamma/\Gamma_\infty)\Gamma, \tag{10}$$

where β and α are the kinetic constants for adsorption and desorption, and K is a measure of (net) attractive or repulsive interactions between the adsorbed surfactants, which are assumed here to alter the desorption kinetics of the surfactant. These parameters can be described in terms of the zero-coverage kinetic constants, β_o and α_o, and the activation energies for adsorption and desorption, E_{ads} and E_{des}, according to

$$\beta = \beta_o \exp\left\{\frac{-E_{ads}(\Gamma)}{RT}\right\}, \tag{11a}$$

$$\alpha = \alpha_o \exp\left\{\frac{-E_{des}(\Gamma = 0)}{RT}\right\}, \quad K = \frac{\partial E_{des}}{\partial \Gamma}(\Gamma = 0). \tag{11b}$$

Surfactants adjacent to the interface adsorb, depleting the concentration in the region exterior to the bubble ($r > b$). Surfactant diffuses toward this depleted region according to Fick's law,

$$D\frac{1}{r^2}\frac{\partial}{\partial r}\left(r^2\frac{\partial C}{\partial r}\right) = \frac{\partial C}{\partial t}, \tag{12}$$

where D is the surfactant diffusivity. This equation obeys two boundary conditions; the sublayer concentration is determined by the diffusion flux according to Equation (8), and the far-field condition requires that

$$\lim_{r\to\infty} C(r,t) = C_\infty. \tag{13}$$

A surface mass balance at the interface requires that diffusion and kinetic fluxes balance, *i.e.*,

$$\frac{d\Gamma}{dt} = D\left(\frac{\partial C}{\partial r}\right)_{r=b}. \tag{14}$$

At equilibrium, the bulk concentration becomes uniform, and the net adsorption–desorption flux becomes zero, yielding the Frumkin adsorption isotherm by equating the right-hand side of Equation (10) to zero:

$$\frac{\Gamma}{\Gamma_\infty} = \frac{C_s/a}{\exp(K\Gamma/\Gamma_\infty) + C_s/a}, \tag{15}$$

where $a = \alpha/\beta$. Corresponding to this isotherm, the surface equation of state relating the surface tension, γ, to the surface concentration, Γ, is given by

$$\gamma = \gamma_o + RT\Gamma_\infty\left[\ln\left(1-\frac{\Gamma}{\Gamma_\infty}\right) - \frac{K}{2}\left(\frac{\Gamma}{\Gamma_\infty}\right)^2\right], \tag{16}$$

where γ_o is the surface tension of the interface in the absence of surfactant adsorption. This expression relates γ_{eq} to the equilibrium surface concentration, Γ_{eq}. In addition, this equation applies far from equilibrium, so Equation (16) is adopted to relate the instantaneous surface concentration, Γ(t), to the instantaneous surface tension, γ(t), in the ensuing dynamic surface-tension simulations.

Mixed Controlled Desorption from a Suddenly Compressed Surface

Consider a bubble at rest with an interface in equilibrium with the bulk concentration. At $t = 0$, let the bubble surface area be reduced, compressing the surface concentration to some value Γ_0 in excess of

Γ_{eq}. For mixed kinetic–diffusion-controlled transport, the surfactant must desorb before it can diffuse away from the interface, and the interface and sublayer concentration are initially out of equilibrium. For these circumstances, the initial condition on the surface concentration (Equation (9)) must be amended to be:

$$C_s(t=0) = C_\infty, \quad C(r, t=0) = C_\infty, \quad \Gamma(t=0) = \Gamma_0. \tag{17}$$

The remaining governing equations and boundary conditions remain unchanged.

Diffusion-Controlled Mass Flux

If adsorption–desorption kinetics are instantaneous, the sublayer concentration, C_s, remains in equilibrium with the instantaneous surface concentration, $\Gamma(t)$, as expressed by the adsorption isotherm in Equation (15). Thus, Equations (12)–(14) are solved simultaneously with Equation (15), subject to the initial conditions

$$C_s(t=0) = C_s(\Gamma_0), \quad C(r, t=0) = C_\infty, \quad \Gamma(t=0) = \Gamma_0. \tag{18}$$

Kinetically Controlled Adsorption/Desorption

If diffusion is rapid compared with adsorption–desorption kinetics, the sublayer concentration is equal to the bulk concentration, and the evolution of the surface concentration is governed by Equation (10) with $C_s = C_\infty$, subject to the initial condition that $\Gamma(t=0) = 0$ for adsorption to a clean interface, or $\Gamma(t=0) = \Gamma_0$ for desorption from a suddenly compressed interface.

Dimensional Analysis of the Governing Equations

Equations (8) and (12)–(14) can be solved analytically to give a closed-form expression relating the surface concentration, $\Gamma(t)$, and sublayer concentration, C_s, in a transcendental equation analogous to the Ward and Tordai equation [15], which can be solved numerically at the interface with the kinetic flux expression to yield the time evolution of Γ and C_s:

$$\Gamma(t) = \Gamma(t=0) + \frac{2}{\sqrt{\pi}}\left\{ C_\infty\sqrt{Dt} - \int_0^{\sqrt{t}} C_s(t-\tau)d\sqrt{D\tau} \right\} + \frac{D}{b}\left\{ C_\infty t - \int_0^t C_s(t')dt' \right\}. \tag{19}$$

We are interested in discussing the effects of decreasing bubble radius on the diffusion mass flux and on the bulk concentration profile, $C(r,t)$. Therefore, we forego this usual approach and solve the bulk equations directly numerically.

All of these equations can be cast in dimensionless form (and indeed are rearranged for the purposes of numerical integration). However, the important dimensional arguments used to guide this study can be made by considering Equations (10) and (19). Adopting the following characteristic scales:

$$\hat{\Gamma} = \frac{\Gamma}{\Gamma_{eq}}, \quad \hat{C} = \frac{C(t)}{C_\infty}, \quad \hat{t} = \frac{t}{\tau_{Dsphere}}. \tag{20}$$

Equation (19) becomes

$$\hat{\Gamma}(\hat{t}) = \frac{2}{\sqrt{\pi}}\frac{b}{h}\left\{\sqrt{\hat{t}} - \int_0^{\sqrt{\hat{t}}} \hat{C}_s(\hat{t}-\hat{\tau})d\sqrt{\hat{\tau}}\right\} + \left\{\hat{t} - \int_0^{\hat{t}} \hat{C}_s(t')dt'\right\}, \tag{21}$$

and the adsorption–desorption flux expression in Equation (10) becomes

$$\frac{d\hat{\Gamma}}{d\hat{t}} = \Omega\left\{\frac{\beta C_\infty}{\alpha}\hat{C}_s\left(\frac{\Gamma_\infty}{\Gamma_{eq}} - \hat{\Gamma}\right) - \hat{\Gamma}\exp\left(-\frac{K\Gamma_{eq}}{\Gamma_\infty}\hat{\Gamma}\right)\right\}, \tag{22a}$$

where

$$\Omega = \frac{\alpha b}{D}\frac{\Gamma_{eq}}{C_\infty} = \Lambda_{sphere}\left(1 - \frac{\Gamma_{eq}}{\Gamma_\infty}\right)\exp\left(-K\frac{\Gamma_{eq}}{\Gamma_\infty}\right). \tag{22b}$$

In these equations, the time scales and dimensionless groups discussed in the Introduction to this article emerge. In Equation (21), the first two terms correspond to the solution for diffusion-controlled adsorption to a planar surface. They are weighted by the ratio of $(h/b)^{-1}$. The second two terms correspond to the effects of curvature on the mass flux. For small radii, $(h/b)^{-1}$ tends to zero, and the planar terms become small corrections to the curvature terms. When the radius is large, $(h/b)^{-1}$ is greater than unity, and the planar terms dominate the solution. (In fact, the appropriate time scale changes from $\tau_{\text{D sphere}}$ to $\tau_{\text{D planar}}$ in that circumstance, and the curvature terms become weak corrections to the planar solution.) In Equation (22), Ω is proportional to Λ_{sphere}. The smaller is Λ_{sphere}, the slower is the kinetic flux to the interface relative to diffusion, and the more important the kinetic barriers to adsorption–desorption become.

Numerical Integration

The governing equations were integrated adopting the constants obtained by Pan *et al.* [6] in their analysis of $C_{12}E_6$; these constants are given in Table 2. The numerical techniques adopted to solve the governing equations are quite standard [16] and so are described only briefly. The bulk mass balance in Equation (12), the diffusion flux to the interface in Equation (14), and the adsorption–desorption flux in Equation (10) are coupled through the sublayer concentration, C_s, and therefore were solved simultaneously. The equations and boundary conditions were discretized using a centered difference scheme with time advanced implicitly. For each time step we use the following iteration scheme. Values for C_s and Γ were taken from the previous iteration step. Equation (12) was solved by the TriDiagonal Matrix Algorithm (TDMA). Equations (10) and (14) were then solved to update C_s and Γ. These iterations were continued until the computed C_s and Γ did not change to within a relative error of 10^{-3}. The next time step was then computed. The length scale for each run was related to h/b; the radial discretization was on the order of 30 grids per that length, and 20 times that length is used for simulating the far-field domain in Equation (13). A time step of 10^{-7} proved to be adequate for all runs. For the kinetic-controlled limit, the mass flux (Equation (10)) was solved for Γ using first-order integration in time, with time steps of 10^{-8}.

RESULTS AND DISCUSSION

The surface concentration and surface tension evolutions predicted numerically for $C_{12}E_6$ are reported here. First, adsorption to an initially surfactant-free bubble is studied for fixed concentration as a function of bubble radius. For radii that are small enough, it is shown that the mass transfer is kinetically controlled for all concentrations. Second, desorption from a surface that is suddenly compressed above its equilibrium surface concentration is studied as a function of decreasing bubble radius at fixed bulk concentration.

In Figures 1a–1c, the equilibrium surface tension, the adsorption isotherm, and the adsorption depth variation with C_∞ that correspond

TABLE 2 $C_{12}E_6$ Frumkin Isotherm Constants

α (s^{-1}) $\times 10^4$	$\beta\Gamma_\infty$ (m/s) $\times 10^5$	Γ_∞ (mol/m^2) $\times 10^6$	K	D (m^2/s) $\times 10^{10}$
1.40	1.40	3.48	6.652	6.00

to the coefficients in Table 2 are shown. In the experiments of Pan *et al.* [6], these constants were established two ways. Equilibrium surface tensions as a function of bulk concentration were obtained as long-time asymptotes to pendant bubble evolutions. These equilibrium data must agree with the adsorption isotherm predictions. A more stringent set of data was obtained by using the pendant bubble as a Langmuir trough. The pendant bubble was formed and equilibrated in a surfactant solution. The bubble interface was then rapidly expanded and compressed, faster than adsorption–desorption or diffusion kinetics could change the adsorbed amount of surfactant. The surface tension variation with surface concentration was measured and compared favorably with the Frumkin model.

Adsorption to an Initially Surfactant-free Spherical Surface

In Figures 2a and 2b, the predicted surface tension and surface concentration evolutions for adsorption to a freshly formed bubble surface for $C_\infty = 8 \times 10^{-7}$ M and $b = 10^{-3}$ m are presented ($h/b = 2.1$). Three curves are shown in each figure. The solid curve corresponds to the full solution of the mixed kinetic–diffusion-controlled model. The dashed curve corresponds to the kinetic-controlled model, and the dashed-dotted curve corresponds to the diffusion-controlled curve.

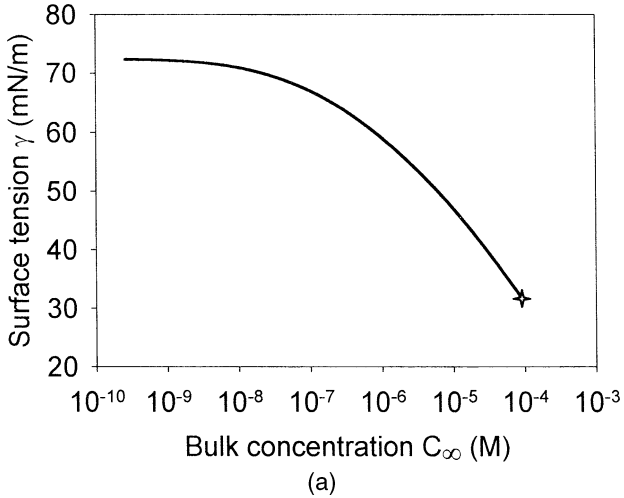

FIGURE 1 (a) The equilibrium surface tension, γ, as a function of bulk concentration, C_∞, using the Frumkin coefficients for $C_{12}E_6$ reported in Table 2. The symbol indicates the CMC at 8.9×10^{-5} M. (b) The corresponding equilibrium adsorption isotherm Γ_{eq} *versus* C_∞. (c) The adsorption depth h *versus* C_∞.

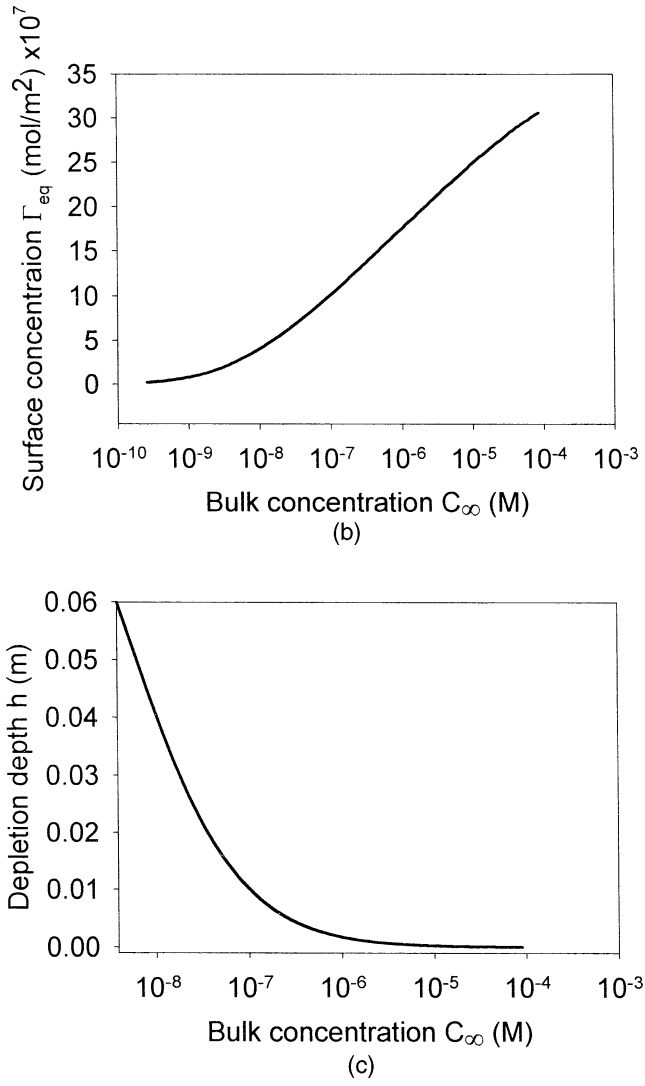

FIGURE 1 (Continued).

In Figures 2a and 2b, the full solution deviates only slightly from the diffusion-controlled prediction. These evolutions are similar to those that were measured at dilute bulk concentrations for $C_{12}E_6$ using the pendant bubble.

In Figure 2, the mixed-controlled predictions are always slower than either the kinetic-controlled predictions or the diffusion-

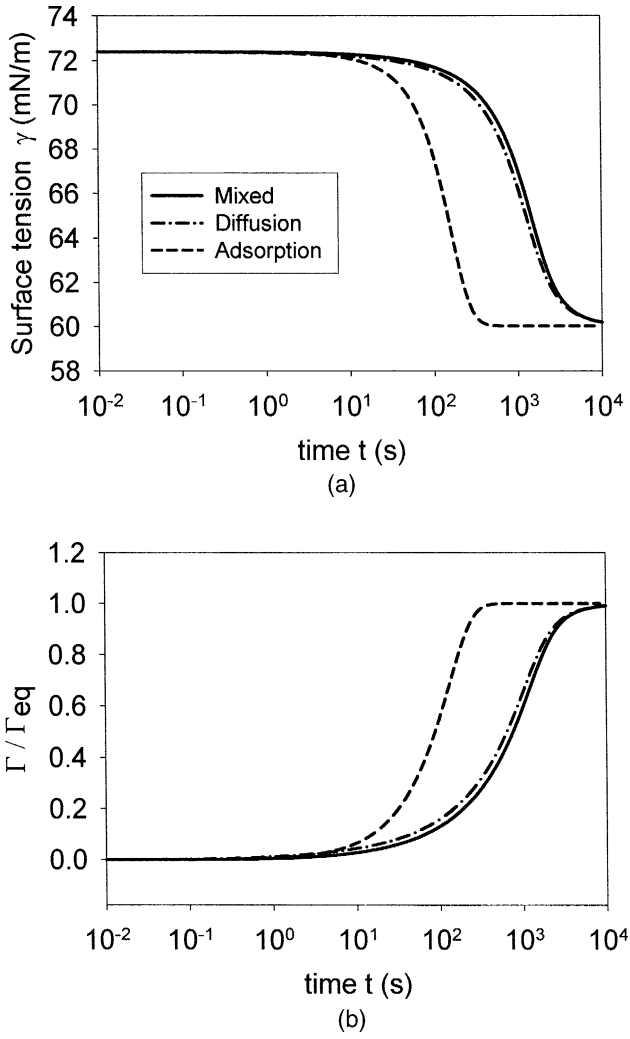

FIGURE 2 (a) The predicted surface tension evolution, $\gamma(t)$, for adsorption to a freshly formed bubble surface. Solid curve: full mixed kinetic–diffusion-controlled model. Dot-Dashed curve, the diffusion-controlled model; dashed curve, kinetic-controlled model. $C_\infty = 8 \times 10^{-7}$ M, $b = 10^{-3}$ m, $h/b = 2.1$. (b) The predicted surface concentration evolution $\Gamma(t)/\Gamma_{eq}$ for the conditions in (a), where $\Gamma_{eq} = 1.68 \times 10^{-6}$ mol/m^2. The full solution deviates only slightly from the diffusion-controlled prediction.

controlled predictions, because the mixed model includes both processes occurring in series. If one of these two processes were rate limiting, the mixed-controlled curve would tend to that rate-limiting

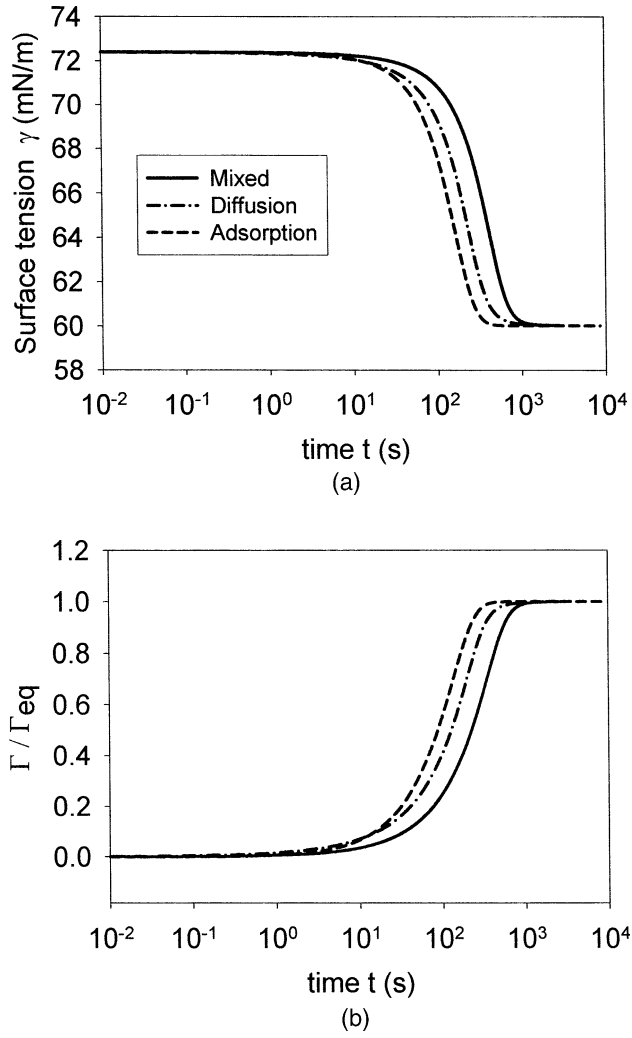

FIGURE 3 (a) The predicted surface tension evolution, $\gamma(t)$, for adsorption to a freshly formed bubble surface. Conventions for model curves are the same as in Figure 2. C_∞ is the same as in Figure 2. $b = 10^{-4}$ m, $h/b = 21$. (b) The predicted surface concentration evolution $\Gamma(t)/\Gamma_{eq}$ for the conditions in (a). The full mixed control solution deviates significantly from the diffusion-controlled prediction.

profile. The aim of this study is to show that the mixed-controlled curve tends to the kinetically-controlled limit as the bubble radius is decreased.

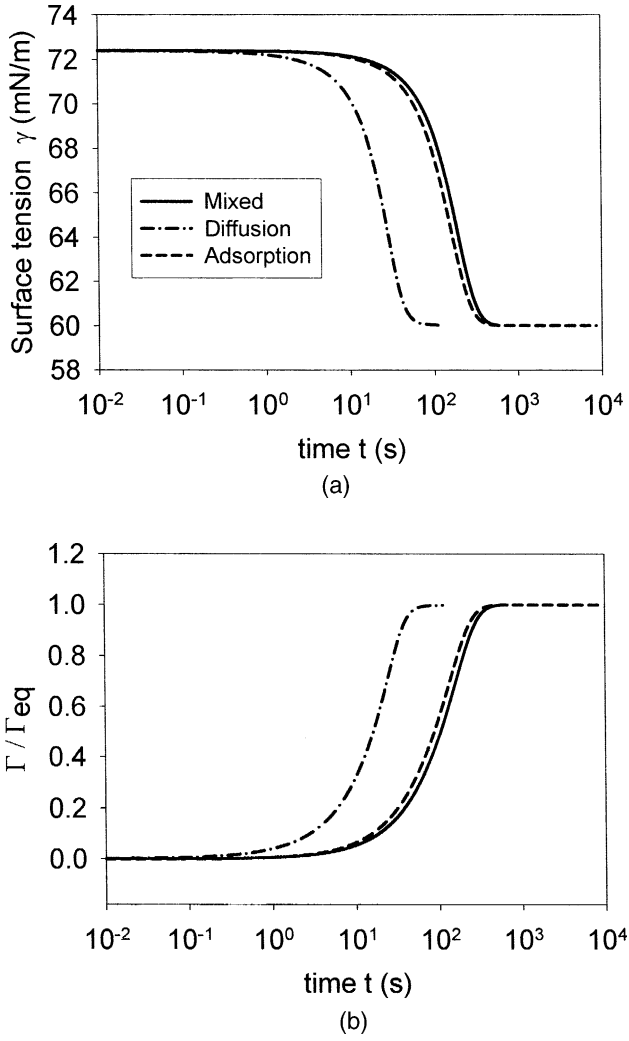

FIGURE 4 (a) The predicted surface tension evolution, $\gamma(t)$, for adsorption to a freshly formed bubble surface. Conventions for model curves the same as in Figure 2. C_∞ is the same as in Figure 2. $b = 10^{-5}$ m, $h/b = 210$. (b) The predicted surface concentration evolution $\Gamma(t)/\Gamma_{eq}$ for the conditions in (a). The full mixed-control solution closely approaches the kinetic-controlled prediction.

Predicted surface tension and surface concentration evolutions in Figure 3a and 3b for $b = 10^{-4}$ m ($h/b = 21$), and in Figures 4a and 4b for $b = 10^{-5}$ m ($h/b = 210$) for fixed $C_\infty = 8 \times 10^{-7}$ M. The profiles move progressively away from the diffusion-controlled limit toward the kinetic-controlled limit as the bubble radius decreases, in agreement with the arguments presented in Equation (7).

This is an intriguing result because the adsorption depth, h, is orders of magnitude larger than the radius of the sphere, indicating that depletion should be significant, and bulk diffusion should play a role in the dynamics of this process. A family of curves for the concentration, C(r), at several time steps for a diffusion-controlled process is presented in Figure 5 for the smallest radius, $b = 10^{-5}$ m. These profiles have similar features for all of the radii studied at this concentration; they indicate that the solution is indeed depleted around the sphere over large distances compared with the sphere radius but that these regions are resupplied by bulk diffusion in times comparable with one τ_{Dsphere}. Since τ_{Dsphere} is proportional to the sphere radius, diffusional fluxes are rapid, allowing adsorption–desorption kinetics, which are independent of sphere radius, to become rate limiting.

The scaling argument presented in Equation (7b) and the constants in Table 2 suggest that for this surfactant drops or bubbles with radii less than 40 microns will be kinetically controlled for all surfactant bulk concentrations. In Figure 4, the surface tension and surface

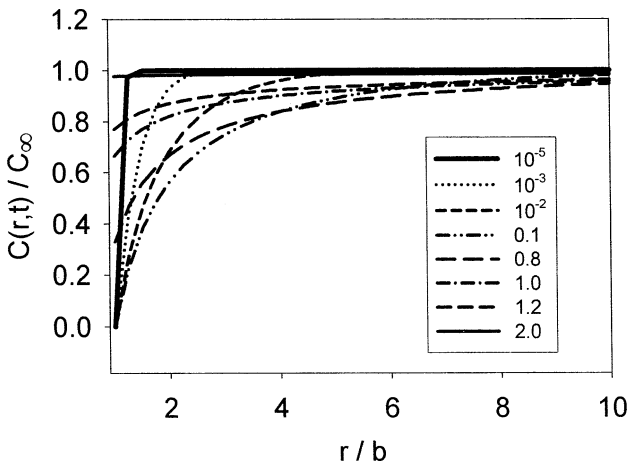

FIGURE 5 The concentration profile in solution, $C(r,t)/C_\infty$, as a function of r/b at several time steps for diffusion-controlled adsorption with $C_\infty = 8 \times 10^{-7}$ M and $b = 10^{-5}$ m. The scaled time (t/τ_{Dsphere}) corresponding to each profile is reported in the figure legend.

concentration evolution for a solution of bulk concentration $C_\infty = 8 \times 10^{-7}$ M and bubble radius 10^{-5} m were shown to agree with kinetically controlled arguments. In Figure 6, the bubble radius is held fixed at 10^{-5} m, while the concentration is decreased by two orders of magnitude. These results show that adsorption to spheres of this radius

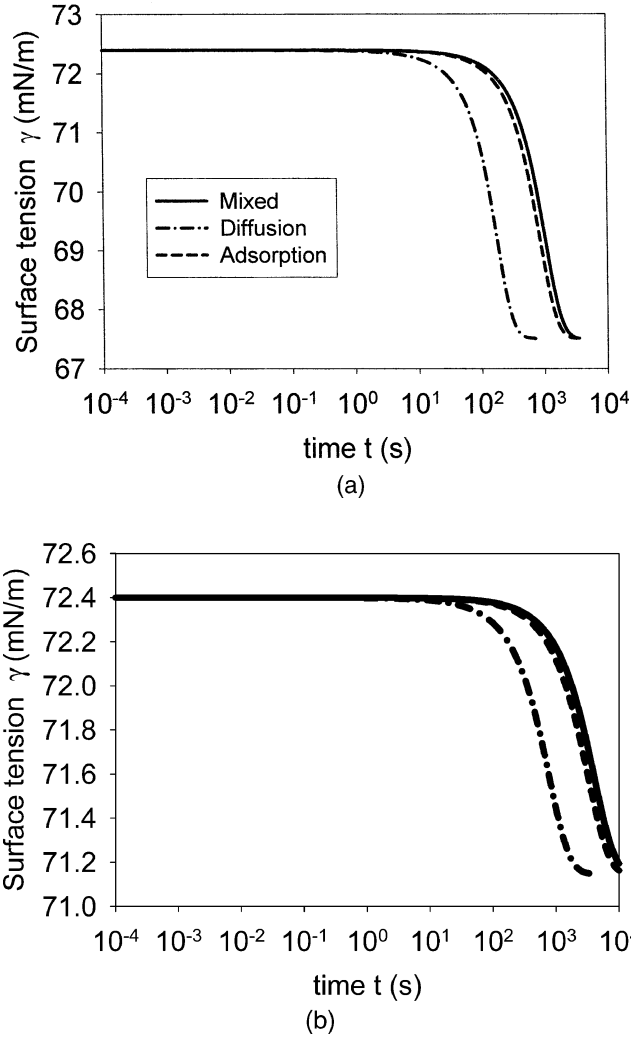

FIGURE 6 γ(t) predictions for $b = 10^{-5}$ m. (a) $C_\infty = 8 \times 10^{-8}$ M; (b) $C_\infty = 8 \times 10^{-9}$ M. Same conventions for model curves as Figure 2. As C_∞ decreases, spheres of this radius remain kinetically controlled.

is kinetically controlled regardless of bulk concentration. Together, the results in Figures 2–6 confirm the shift of mechanism with bubble radius predicted by Equation (7b) for adsorption to an initially surfactant-free interface.

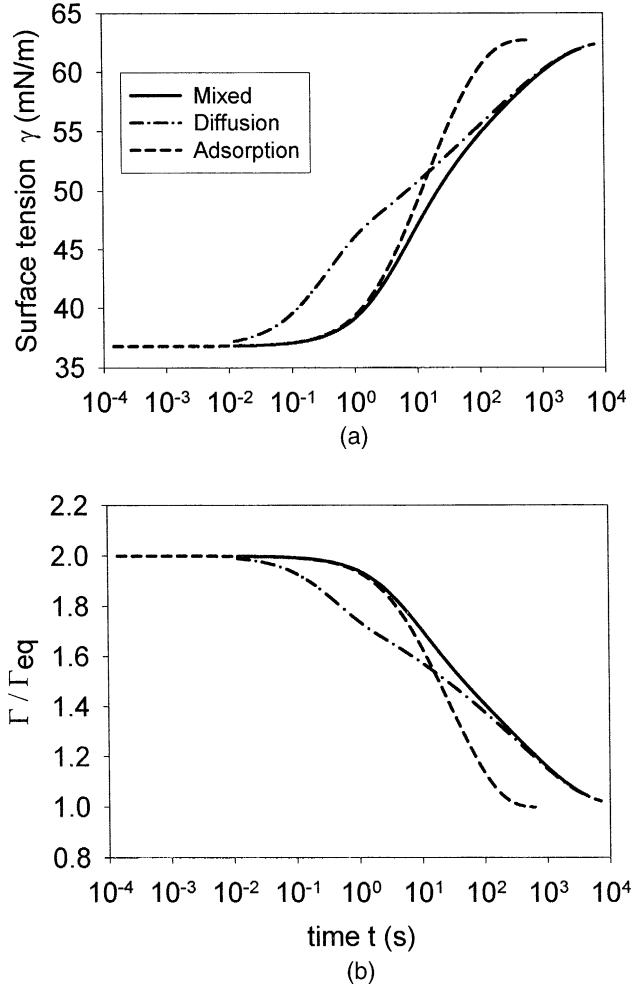

FIGURE 7 The predicted profiles for desorption and diffusion away from a spherical surface compressed so $\Gamma(t=0)/\Gamma_{eq}=2$. $C_\infty = 4\times10^{-7}$ M, $\Gamma_{eq} = 1.45\times10^{-6}$ mol/m^2; $b = 10^{-3}$ m, $h/b = 3.61$. Same conventions for model curves as Figure 2. (a) $\gamma(t)$, (b) $\Gamma(t)/\Gamma_{eq}$. The full mixed-control solution agrees with a kinetically controlled model at early times, diffusion-controlled model at later times.

Desorption from a Compressed, Surfactant-rich Spherical Surface

This shift in controlling the mass transfer mechanism with decreasing bubble radius should also occur for interfaces that are compressed to initial surface concentrations $\Gamma_0 > \Gamma_{eq}$. These experiments are usually

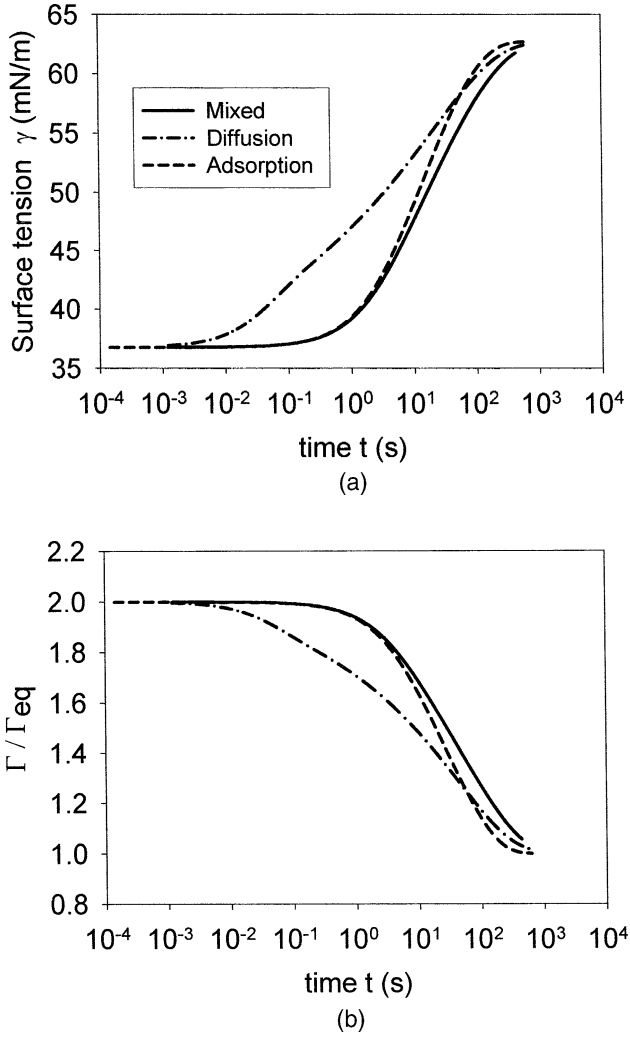

FIGURE 8 Predicted profiles for $b = 10^{-4}$ m, $h/b = 36.1$. All other conditions the same as in Figure 7. (a) γ(t), (b) Γ(t)/Γ_{eq}. The full mixed-control solution agrees with a kinetically controlled model over much of the evolution.

performed at sufficiently dilute concentrations that Γ_0 can be significantly larger than Γ_{eq} yet still remain sufficiently less than the maximum packing limit, $\Gamma_\infty = 3.48 \times 10^{-6}\,\mathrm{mol/m^2}$, so that the surface tension is still large enough to hold the bubble on the needle. In our simulations, we choose a bulk concentration of $C_\infty = 4 \times 10^{-7}\,\mathrm{M}$, with

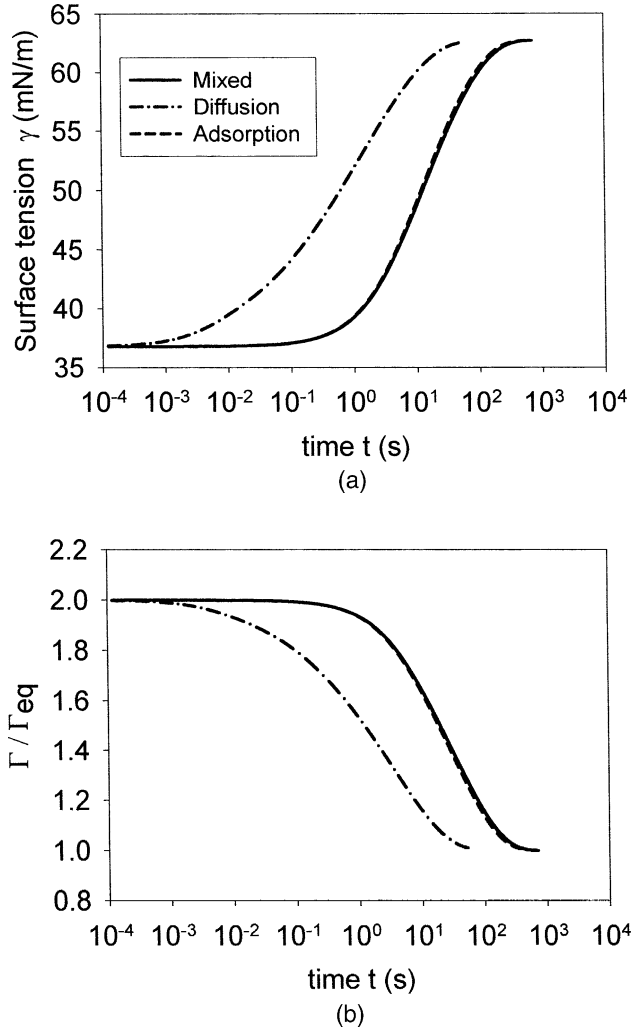

FIGURE 9 Predicted profiles for $b = 10^{-5}\,\mathrm{m}$, $h/b = 361$. All other conditions the same as in Figure 7. (a) $\gamma(t)$, (b) $\Gamma(t)/\Gamma_{eq}$. The full mixed-control solution superposes with the kinetically controlled model.

a corresponding $\Gamma_{eq} = 1.45 \times 10^{-6}\,\mathrm{mol/m^2}$, and study the case of $\Gamma_0 = 2\Gamma_{eq}$.

Surfactant must desorb and diffuse away to re-establish equilibrium. The surface concentration and surface tension evolutions predicted for decreasing radii are presented in Figures 7–9. Again, there are three curves in each figure. For $b = 10^{-3}\,\mathrm{m}$, kinetics control the initial evolution and diffusion controls the late stages of equilibration, as shown in Figures 7a and 7b. For $b = 10^{-4}\,\mathrm{m}$ similar trends are observed, but with smaller discrepancies between the mixed-control model and the kinetically controlled limit, as reported in Figures 8a and 8b. Finally, in Figures 9a and 9b, for which $b = 10^{-5}\,\mathrm{m}$, m, the entire evolution agrees closely with the kinetically controlled model.

CONCLUSIONS

In this article a new intrinsic-length scale, $R_{D\text{-}K}$, was developed to describe adsorption to spherical surfaces. This length scale is significant for adsorption to curved surfaces, for which the ratio of the adsorption depth, h, to the drop or bubble radius, b, is large. For all drops or bubbles with radii larger than $R_{D\text{-}K}$, mass transfer to the surface is diffusion controlled. For all drops or bubbles with radii less than $R_{D\text{-}K}$, mass transfer is kinetically controlled. Significantly, $R_{D\text{-}K}$ is independent of bulk concentration, so drops or bubbles that have adsorption–desorption controlled mass transfer will be kinetically controlled regardless of how dilute the solution. For highly surface-active compounds, $R_{D\text{-}K}$ is on the order of tens of microns. These results indicate that new surface analysis techniques for the study of dynamic surface tension at reduced length scales should allow significant progress in the study of adorption–desorption barriers.

REFERENCES

[1] Rotenberg, Y., Boruvka, L., and Neumann, A. W., *J. Colloid Interface Sci.* **93**, 169–183 (1983).
[2] Chang, C.-H. and Fanses, E., *Colloids Surf. A: Physicochem. Eng. Aspects* **100**, 1–45 (1995).
[3] Miller, R., Joos, P., and Fainerman, V., *Adv. Colloid Interface Sci.* **49**, 249–302 (1994).
[4] Dukhin, S. S., Kretzschmar, G., and Miller, R., *Dynamics of Adsorption at Liquid Interfaces* (Elsevier, Amsterdam, 1995).
[5] Ferri, J. K. and Stebe, K. J., *Adv. Colloid Interface Sci.* **85**, 61–97 (1999).
[6] Pan, R. N., Green, J., and Maldarelli, C., *J. Colloid Interface Sci.* **205**, 213–230 (1998).

[7] Lee, Y. C., Stebe, K. J., Liu, H.-S., and Lin, S. Y., *Colloids and Surfaces A—Physicochem. Eng. Aspects* **220**, 139–150 (2003).
[8] Lin, S. Y., Tsay, R. Y., Lin, L. W., and Chen, S. I., *Langmuir* **12**, 6530–6536 (1996).
[9] Tsay, R. Y., Lin, S. Y., Lin, L. W., and Chen, S. I., *Langmuir* **13**, 3191–3197 (1997).
[10] Chang, H. C., Hsu, C. T., and Lin, S. Y., *Langmuir* **14**, 2476–2484 (1998).
[11] Stone, H. A. and Kim, S., *AICHE J.* **47**, 1250–1254 (2001).
[12] Ferri, J. K., Lin, S. Y., and Stebe, K. J., *J. Colloid Interface Sci.* **241**, 154–168 (2001).
[13] Ferri, J. K. and Stebe, K. J., *Colloids Surf.* **156**, 567–577 (1999).
[14] Frumkin, A., *Zeitschrift fur Physikalische Chemie-Leipzig* **116**, 466–484 (1925).
[15] Lin, S. Y., McKeigue, K., and Maldarelli, C., *AIChE J.* **36**, 1785–1795 (1991).
[16] Patankar, S. V., *Numerical Heat Transfer and Fluid Flow* (Hemisphere Publishing, New York, 1980).